IOP Publishing Plasma Physics and Controlled Fusion
Plasma Phys. Control. Fusion **62** (2020) 055015 (10pp) https://doi.org/10.1088/1361-6587/ab831b

The erosion of tungsten divertor on EAST during neon impurity seeding in different divertor operation regimes

Xuele Zhao[1], Chaofeng Sang[1], Qingrui Zhou[1], Chen Zhang[1], Yanjie Zhang[1], Rui Ding[2], Fang Ding[2] and Dezhen Wang[1]

[1] School of Physics, Dalian University of Technology, Dalian 116024, People's Republic of China
[2] Institute of Plasma Physics, Chinese Academy of Sciences, Hefei 230031, People's Republic of China

E-mail: sang@dlut.edu.cn

Received 30 November 2019, revised 22 March 2020
Accepted for publication 25 March 2020
Published 20 April 2020

Abstract

The external Ne impurity seeding has been applied to reduce the heat flux to the divertor target as well as plasma temperature to prolong the lifetime of the EAST upper tungsten (W) target. The erosion of the W target during the Ne seeding in different divertor operation regimes has been assessed by using the semi-empirical formula, while the plasma background was provided by SOLPS modeling. The simulation results showed that the Ne impurity played a critical role in the W erosion, which depended strongly on the operation regimes. By increasing the Ne seeding rate, the discharge regime was varied from the attached to detached condition. During the attached regime, the insufficient seeded Ne impurity could reduce the heat flux to the target, but the erosion of the W target was obviously enhanced, which may shorten the target lifetime. By the sufficient impurity seeding, the detached condition could be achieved, and the W target erosion was obviously suppressed. The high-power discharge brings great challenge to the W target lifetime, and the erosion is mainly induced by Ne and D ions. The contribution of each species changes greatly with different Ne seeding rates. In addition, the lifetime of the EAST upper W divertor has also been evaluated in different operation regimes during high input power discharge.

Keywords: tokamak, tungsten divertor, neon seeding, erosion

(Some figures may appear in colour only in the online journal)

1. Introduction

The application of tungsten (W) as the plasma-facing materials (PFMs) has been widely accepted by different tokamaks, due to its favorable properties such as high melting temperature, high thermal conductivity, low sputtering yields, and low fuel retention rate [1–4]. Pure W is chosen as the PFM of the ITER divertor (dome and both targets) [5]. Since the high plasma temperature in the core (thousands eV) is required to satisfy the deuterium (D)-tritium (T) fusion reaction requirement, the plasma wall interactions (PWI) becomes to a great concern for the PFMs protection during high-performance long-pulse discharges [6]. Moreover, W is a very strong radiator in the plasma temperature relevant to the core plasma, thus the central concentration of W impurity must be kept at or below 10^{-5} to avoid the loss of plasma operation and performance [7]. The W impurities are mainly produced by the erosion of (1) the divertor by the intense plasma flux [8] and (2) the first wall by the energetic particles [9, 10].

To prolong the lifetime of the W divertor and suppress the W erosion, it is required not only to reduce the power load to the target (<10 MW m^{-2}), but also to cool down the temperature of plasma near the target [11, 12]. The radiative divertor operation is a good method to raise the divertor energy dissipation, thus reduce heat flux to the target. Due to the plasma density is limited by the current, it is hard to achieve

detached plasma by only increasing the central plasma density. The external gas seeding, such as argon (Ar), neon (Ne) or nitrogen (N), is the alternative method [13]. The application of Ne seeding has been proposed and studied on ITER, showing the advantages of power radiation and impurity control [14]. However, the external noble gas seeding may make the erosion of W PFMs at the divertor more complicated. As we know that the W sputtering yield depends strongly on the incident particle species and their energies, the introduced Ne to W has much lower sputtering energy threshold than that of D, and for the same incident energy, Ne has much higher sputtering yield than that of D. This indicates that the lifetime of W target will be threatened more seriously by seeding impurity than the fuel particle [15–18]. Therefore, it is important to understand the erosion of W divertor target during the impurity gas seeding in different divertor operation regimes.

EAST is a fully superconducting divertor tokamak with D-shaped poloidal cross-section. The upper divertor of EAST has been upgraded to use ITER-like mono-block W PFM in 2014. Now, W and carbon (C) is, respectively, used as PFMs of upper and lower divertor on EAST [19]. Our previous work [11] reported that on EAST C impurity produced at the lower graphite targets could transport to the upper W targets and cause the W erosion. The concentration of the C density at the upper divertor region is low, and thus, the W erosion rate by C impurities is small. However, during the high power discharge, the erosion of W by D particle becomes to a serious problem, and the erosion of EAST W divertor with the impurity gas seeding remains unsolved.

In this work, the erosion of upper W divertor on EAST during the Ne injection in different divertor operation regimes has been assessed. The two-dimensional code package SOLPS [20] has been applied to provide the divertor plasma background, and the erosion of the W divertor has been calculated by using the semi-empirical formula [15–17]. The erosion of W, by D^+, carbon ions and Ne ions, was considered. The power across the separatrix was varied from 1.5 MW to 8.0 MW to simulate from the low power to high power discharges. Under the same input power and core-edge-interface (CEI) D^+ density conditions, by only varying the Ne seeding rate, the divertor operation regime was changed from the attached to detached. The erosion of W during different conditions by different particles has been analyzed, and the lifetime of the W target has also been discussed according to the calculation.

2. Simulation model

2.1. The divertor plasma simulation

In the present work, the SOLPS5.0 code package is used to simulate the divertor plasma parameters [20]. The D, C, Ne with all charge states are considered. The electrons and ions are handled by B2.5, and neutral particles (D, C, Ne and D_2) are traced by EIRENE [20, 21]. The atomic and molecular processes including ionization, charge exchange, dissociation, elastic collisions, and volume recombination process are included, which is similar to [22]. The setups of the boundary

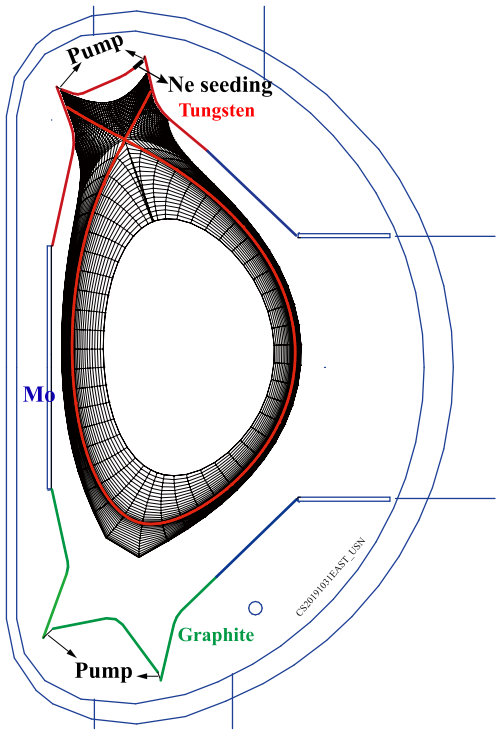

Figure 1. SOLPS simulation mesh for EAST USN configuration. The plasma-facing materials, neon gas seeding and pumps are marked in the sketch.

conditions, and radial transport coefficients are the same to our previous work [11, 23, 24].

The typical upper-single null (USN) magnetic field configuration of EAST is used, as shown in figure 1. EAST has the graphite lower divertor targets and W upper divertor targets, and the main chamber PFCs (first wall) is molybdenum (Mo). The reflection of D on different materials plays important role in the divertor plasma, and the reflection rates in this work are identical to [25]. The input power P_{SOL} and D^+ density at the core boundary of the modeling grid (e.g. r-r_{sep} at the outer mid-plane (OMP) ~6.6 cm) are fixed. For the graphite PFCs, the physical sputtering yield Y_{phys} is calculated by the modified Roth-Bohdansky formula, while the chemical sputtering yield is fixed to 0.01. The eroded W and Mo impurities are not included. The Ne atoms are injected from upper outer divertor region as shown in figure 1. Four pumps are set at the corner of each divertor with the recycling rate fixed to 0.8. Lithium (Li) coating has been widely applied to EAST experiment, which made the PWI much more complicated. It has been reported in [26]. that with Li coating, the low Z impurities can be significantly suppressed; at the meanwhile, the effective W sputtering by Li impurity is low. In the future devices such as CFETE and ITER, Li will not coexist with W PFCs; therefore, Li impurity is neglected in the present work. Other impurities such as N and O are not included due to their low content.

In the current simulation, the input power varies from 1.5 MW to 8.0 MW, and the D^+ density at the CEI is fixed

to 3.5 × 10^{19} m^{-3}. The Ne puffing rate changes from 0.0 to 2.0 × 10^{20} Ne atoms/s. Due to the numerical difficulty, drifts are not included. Only steady-state condition is simulated and the ELMs condition is not taken into consideration.

2.2. The tungsten erosion calculation

When the particle hits the wall, if the material lattice atom gets enough momentum which can overcome surface binding energy, physical sputtering occurs [27]. Therefore, there exists a sputtering threshold energy. The energy and angular dependence of physical sputtering yield for W ($Y_{phy,w}$) with different incident ions can be calculated by using semi-empirical formula [15–17]:

$$Y^{phy}(E_0) = QS_n(\varepsilon)[1-(E_{th}/E_0)^{2/3}](1-E_{th}/E_0)^2(cos\alpha)^{-f} exp\{f[1-(cos\alpha)^{-1}]cos\alpha_{opt}\} \quad (1)$$

The definition of each quantities and more details can be found in [28]. The W erosion rate is expressed as

$$\frac{R_{Ero}S\rho}{M}N_A = Y_{phy,W}\Gamma S \quad (2)$$

and equation(2) can be derived to

$$R_{Ero} = Y_{phy,W}\Gamma M/(\rho N_A) \quad (3)$$

where R_{Ero} represents the W erosion rate, M and ρ is atomic mass and density of W, respectively, N_A is the Avogadro's constant, Γ is the incident particle flux density and S is the area of the target [29]. The erosion rate in equations (2) and (3) is one dimension, and the direction is assumed to be perpendicular to the target.

In this work, to calculate $Y_{phy,w}$, an averaged incidence angle of 45° is assumed [11]. The incident energy dependences of $Y_{phy,w}$ for bombardment with D, C and Ne are shown in figure 2. It can be seen that $Y_{phy,w}$ increases as the incident energy increases once the energy exceeds the energy threshold. The energy threshold for W, with D, C and Ne is about 220 eV, 50 eV and 38 eV, respectively [27, 30–32]. For the same incident energy, heavier ion has larger $Y_{phy,w}$ than that of lighter ion, e.g. the $Y_{phy,w}$ with C and Ne is much larger than with D.

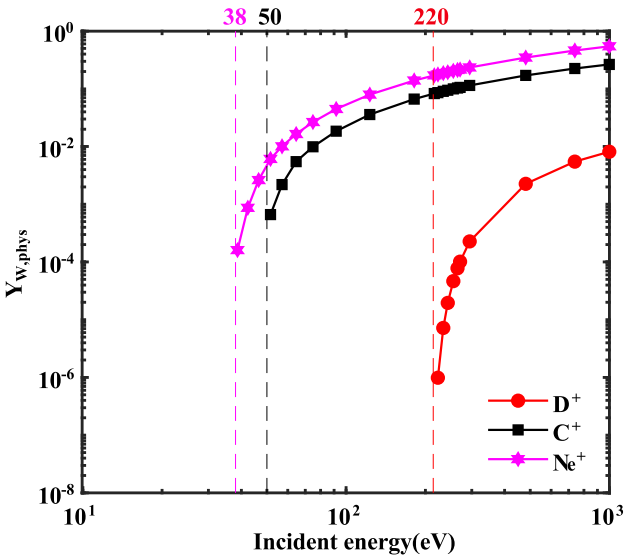

Figure 2. Energy dependence of physical sputtering yield of W ($Y_{phy,w}$) for bombardment with D, C and Ne. The incident angle is 45°.

3. Simulation results

3.1. The divertor plasma during Ne impurity seeding

The high power long-pulse discharge is necessary for EAST to investigate the steady-state operation, which is required by ITER [33]. This will bring great challenge to the W divertor to dissipate energy and protect the target. The divertor plasma parameters under different power across the separatrix P_{SOL} can be obtained by using SOLPS modeling. Due to the existence of the divertor in-out asymmetry, the outer divertor usually suffers higher heat flux load [34, 35] . We focus on the outer divertor study in this work. The averaged discharge shot number on EAST is about 3000 shots/year, and shot duration is about 60 s (long-pulse)/10 s (shot pulse in averaged). The thickness of the W layer is 5.5 mm from plasma-facing surface (PFS) to the water cooling tube. We assume all the shots belong to long-pulse, and the expected lifetime of the PFM is 15 years, therefore, R_{Ero} should be controlled bellow 2.0 nm s^{-1}. Since ELM, which can significantly increase R_{Ero}, is not included in the present model, the critical erosion rate during the ELM-free period should at least be R_{Ero} < 1.0 nm s^{-1} on EAST. When there is no Ne seeding, figure 3 shows the peak and OSP values of electron temperature (T_e), deposited energy density (q), and the corresponding R_{Ero} as functions of P_{SOL} at the outer target. R_{Ero} is calculated by using equation (3) via sputtering yield and incident flux. It can be seen that T_e and q raises significantly as P_{SOL} increases. When P_{SOL} = 1.5 MW, the peak T_e is about 54 eV, the peak q is ~ 3.4 MW m^{-2}, and the corresponding peak R_{Ero} is only 1.1 × 10^{-3} nm s^{-1}, which is induced mainly by C impurity from the lower graphite target [11]. Both q and R_{Ero} satisfy the divertor requirements, therefore, the additional impurity seeding is not necessary. As P_{SOL} increases to 3.0 MW, the peak T_e raises to about 245 eV. Although q_{peak} ~ 5.7 MW m^{-2} is still below 10 MW m^{-2}, but R_{Ero} increases to as high as 1.8 nm s^{-1}. When P_{SOL} is beyond 5 MW, both the peak q and R_{Ero} exceed the tolerance of W PFMs. Therefore, the external gas seeding to increase the divertor power radiation, thus to reduce both T_e and q, is necessary. It should be noted that the peak value of each parameters does not necessary appear at the same location, therefore, we focus on the OSP analysis unless otherwise stated.

As it is pointed out that the external impurity seeding is necessary during the high power discharge to satisfy both the heat load and W erosion limitation. To illustrate the effects of impurity gas seeding on the divertor plasma, the divertor plasma comparisons between with (Ne seeding rate 6.0 × 10^{19} atoms/s) and without Ne seeding cases are shown

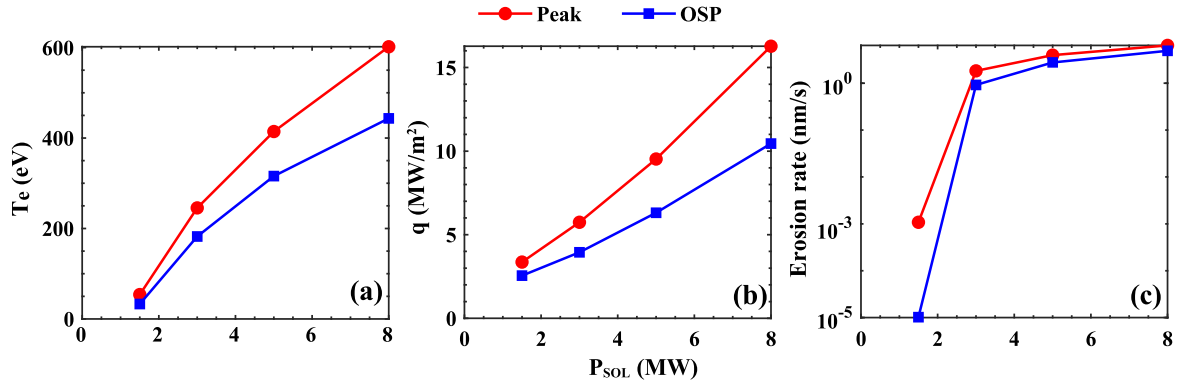

Figure 3. The peak (maximum value) and outer strike point (OSP) values of (a) electron temperature T_e, (b) deposited energy density q, and (c) W erosion rate R_{Ero} at the outer target as functions of P_{SOL} without Ne seeding.

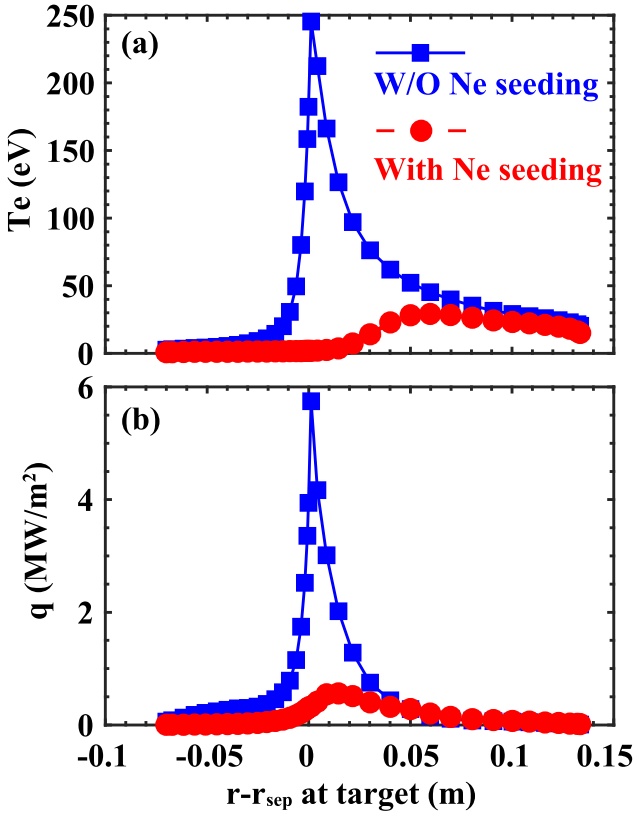

Figure 4. The (a) T_e and (b) heat flux q profiles along the EAST upper outer divertor with (seeding rate is 6.0×10^{19} atoms/s) and without Ne seeding, $P_{SOL} = 3.0$ MW.

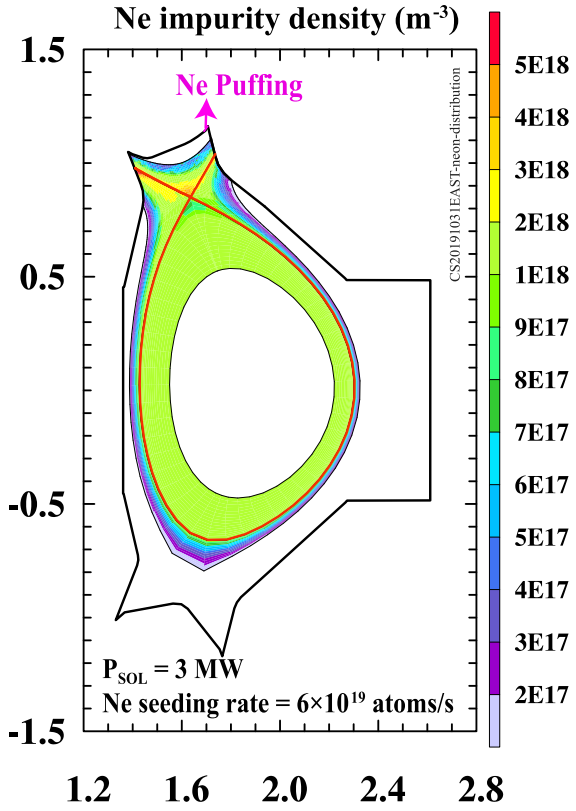

Figure 5. The 2D contour of the total Ne density distribution (sum over all charge states including atom). The input power is $P_{SOL} = 3.0$ MW and Ne seeding rate is 6.0×10^{19} atoms/s.

in figure 4 ($P_{SOL} = 3.0$ MW). It can be seen that by introducing Ne impurity, the peak T_e reduces from ~ 245 eV to ~ 29 eV, peak q falls from ~ 5.7 MW m^{-2} to ~ 0.6 MW m^{-2}. This proves that the Ne seeding can significantly increase the divertor power dissipation, thus the damage risk of the W divertor during the discharge may be greatly reduced. The corresponding total Ne impurity density distribution ($\sum_{n=0}^{n=10} n_{Ne}^{n+}$) in the simulation domain is shown in figure 5, where n_{Ne}^{n+} is the density of Ne with the charge state n. It is clearly that Ne impurity mainly distributes in the divertor and private flux regions. The Ne particles across the separatrix are ionized to the highest charge state, and accumulate in the core region [36]. The highest Ne density appears along the separatrix in the inner and outer divertor regions, which manifests that the vicinity of strike points faces the most intense Ne flux. As a

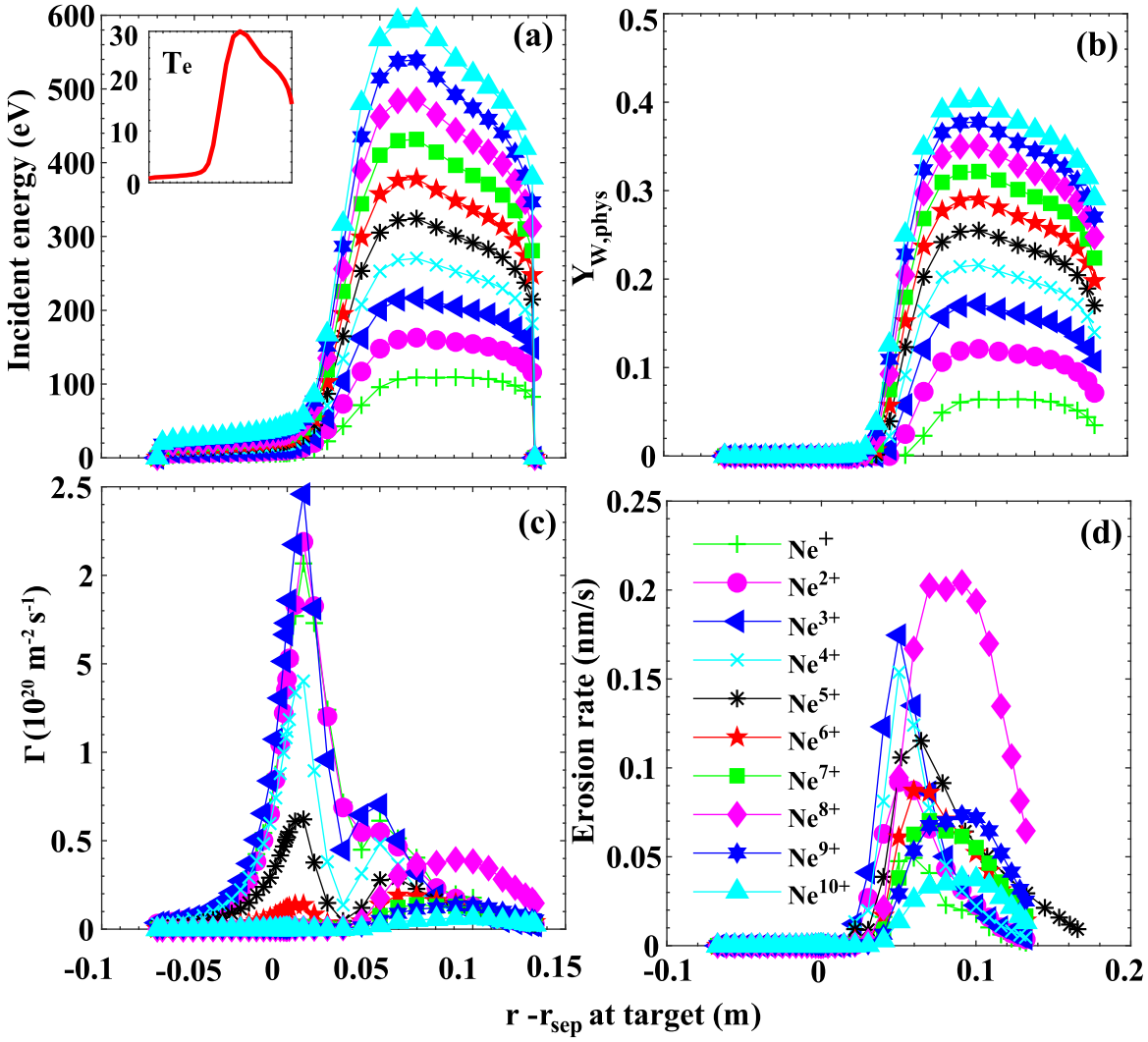

Figure 6. The profiles of (a) the averaged incident energy (the inset-graph is the T_e), (b) calculated W physical sputtering yield, (c) the incident particle flux density, and (d) the W erosion rate, of/by Ne ions with different charge states, at the EAST upper outer divertor target. The input power is P_{SOL} = 3.0 MW and Ne seeding rate is 6.0 × 10^{19} atoms/s.

result, the erosion of the W target by Ne ions may become to a severe problem.

According to figures 3 and 4, it can be found that the power load to the W target can be reduced to below 10 MW m^{-2} without too much difficulty on EAST by external impurity seeding, indicating that the power load handling can be not a major concern. This is in agreement with previous studies [37, 38]. Thus, we mainly focus on the erosion of W target study in the following section.

3.2. The erosion of W divertor during Ne seeding

The semi-empirical formula equation (1), which is a function of incident particle species, incident particle energy and angle, is applied to calculate the physical sputtering yield when the particle hit the W target. The incident angle is fixed to 45° based on the ERO simulation of EAST and DIII-D experiment. To illustrate the calculation of the W target erosion, the plasma condition of figure 5 is chosen, i.e. the P_{SOL} = 3.0 MW and Ne seeding rate 6.0 × 10^{19} Ne atoms/s. Figure 6(a) shows the incident energy of Ne ion with each charge state at the outer W target, and the corresponding T_e along the target can be seen in the inset-graph. The peak T_e is about 29 eV, whereas the peak incident energy of Ne^{+} and Ne^{10+} is about 100 eV and 600 eV, respectively. The ion can be accelerated by the sheath before incident on the target, and the increased energy is $\Delta\varepsilon\Phi z$, where Φ is the sheath potential and z is the charge state. The peak energy of Ne^{n+} is far beyond the W sputtering energy threshold (38 eV), therefore, the physical sputtering occurs [11, 39]. The calculated $Y_{W,phys}$ by Ne ions with each charge state is shown in figure 6(b). Obviously, higher charge state Ne ion leads to larger $Y_{W,phys}$ due to higher incident energy. The peak $Y_{W,phys}$ induced by Ne^{10+} reaches as high as 0.4. The incident Ne ion flux density is presented in figure 6(c), it can be seen that Ne ions with low charge states (1–4) have higher particle flux densities than those of high charge states (5–10), due to that most of low charge state Ne ions exist in the divertor region. The target erosion rate R_{Ero}, which

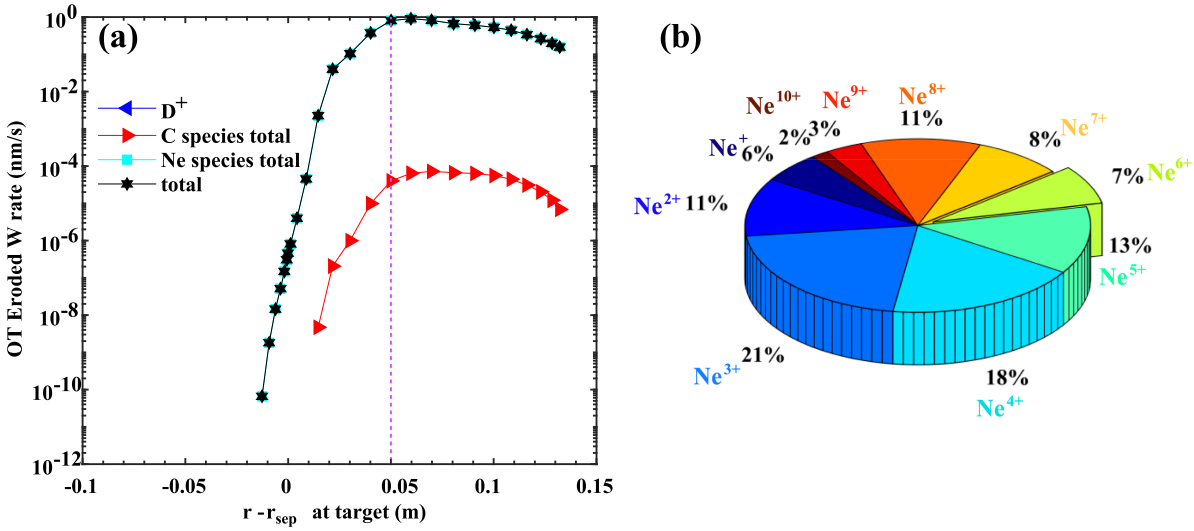

Figure 7. (a) The R_{Ero} by different species along the outer W target, and (b) the contribution of each charge state Ne ions to the total Ne-induced R_{Ero} (the corresponding peak R_{Ero} at r-r_{sep} = 0.05 m as the dash line labeled in figure 7(a)). The input power is P_{SOL} = 3.0 MW and Ne seeding rate is 6.0 × 10^{19} Ne atoms/s.

the product of Γ and $Y_{W,phys}$ can be calculated by equation(3), and is shown in figure 6(d). As can be seen that the peak R_{Ero} ranges from ~ 0.05 nm s^{-1} to ~ 0.22 nm s^{-1}, and Ne^{8+}, Ne^{3+} and Ne^{4+} can lead to the highest W erosion rate. Although Ne^{8+} has lower flux density than those of Ne^{3+}or Ne^{4+}, the incident energy of Ne^{8+} is much larger than Ne^{3+}or Ne^{4+}. Consequently, Ne^{8+} ion gives rise to the biggest threat to the W target (peak R_{Ero} ~ 0.22 nm s^{-1}). It should be noted that the peak $Y_{W,Phys}$ and Γ is not in the same position. The peak $Y_{W,Phys}$ locates in the far OSP region and the peak Γ is closed to the OSP, as a result the location of peak R_{Ero} offsets the OSP.

Summing the W erosion rate ($R_{Ero}^{Ne^{n+}}$) by Ne with each charge state in figure 6(d), the total erosion induced by the Ne ions can be obtained ($R_{Ero}^{Ne} = \sum_{n=1}^{10} R_{Ero}^{Ne^{n+}}$). The erosion rate by D and C species can be calculated via similar method. The total W erosion rate of the outer target is the sum of the three species contribution, i.e. $R_{Ero}^{total} = R_{Ero}^{D} + R_{Ero}^{C} + R_{Ero}^{Ne}$, which is shown in figure 7(a). It can be seen that in this condition, the divertor target was eroded mainly by Ne ions, reaching to ~ 1 nm s^{-1}. The energy of D^+ is below the W sputtering energy threshold (~220 eV) since the peak T_e is only ~29 eV. The content of C is very low [11], therefore, it plays a small role in the W erosion. The peak erosion rate (at the position of r-r_{sep} = 0.05 m) is selected, and the ratio of erosion contributed by different Ne ions is shown in figure 7(b). It is clearly that Ne^{3+} and Ne^{4+} ions lead to the highest ratio of the erosion, which is in agreement with figure 6(d). This result reveals that the seeded impurity becomes to the biggest threat to the W erosion in the attached (or partial detached) plasma operation regime. It drives us to understand the W erosion in different regimes to figure out the best solution regards to the target protection.

The high power discharge is the greatest challenge to the W target lifetime. To fully assess the erosion of the target during the impurity seeding, three input powers, i.e. P_{SOL} = 3.0 MW, 5.0 MW and 8.0 MW, are chosen. By changing the seeding rate, different operation regimes from attached to detached can be obtained as shown in figure 8. The peak T_e is reduced significantly as Ne puffing rate increases, which is in agreement with [36, 40]. When P_{SOL} = 3.0 MW, the peak T_e is ~ 245 eV without Ne seeding, and it falls to 5.8 eV when Ne seeding rate reaches 7.5 × 10^{19} atoms/s. The corresponding peak R_{Ero} decreases from ~ 1.8 nm s^{-1} to 0.05 nm s^{-1}. For P_{SOL} = 5.0 MW, the peak T_e decreases from ~ 415 eV to 4.1 eV as the puffing rate increases from 0 to 1.5 × 10^{20} atoms/s; and the peak R_{Ero} reduces from 3.9 nm s^{-1} to 0.04 nm s^{-1}. During the highest power P_{SOL} = 8.0 MW, the peak T_e reduces from ~ 600 eV to 3.3 eV as the Ne seeding rate reaches 2.0 × 10^{20} atoms/s. The peak R_{Ero} is 6.4 nm s^{-1} without seeding, and falls to 0.033 nm s^{-1} when Ne seeding rate reaches 2.0 × 10^{20} atoms/s. The simulation results demonstrate that the R_{Ero} first increases to a higher value, and then decreases significantly as the seeding rate increases (P_{SOL} = 5.0 and 8.0 MW). The erosion of the W targets depends strongly on the divertor T_e as shown in figure 8(c). To reduce the erosion rate below 1 nm s^{-1}, peak T_e < 18 eV should be satisfied for all three P_{SOL}. Higher P_{SOL} requires lower T_e for the same erosion rate limitation. Only when the incident energy is below the sputtering threshold, the erosion of the target can be fully eliminated. However, the simulation finds that the erosion can be greatly suppressed, but is not fully eliminated even peak T_e < 5 eV [41]. It reveals that higher P_{SOL} requires more impurity to effectively reduce the plasma temperature, and this will face more serious erosion problem.

To explain the variation of peak erosion rate with the Ne seeding rate under different heating power, the composition of total R_{Ero}, which is induced by D, C and Ne, respectively, is presented in figure 9. We can see that the C ions play the negligible role in the target erosion. The total erosion is mainly contributed by D and Ne ions. From equation (3), we can obtain

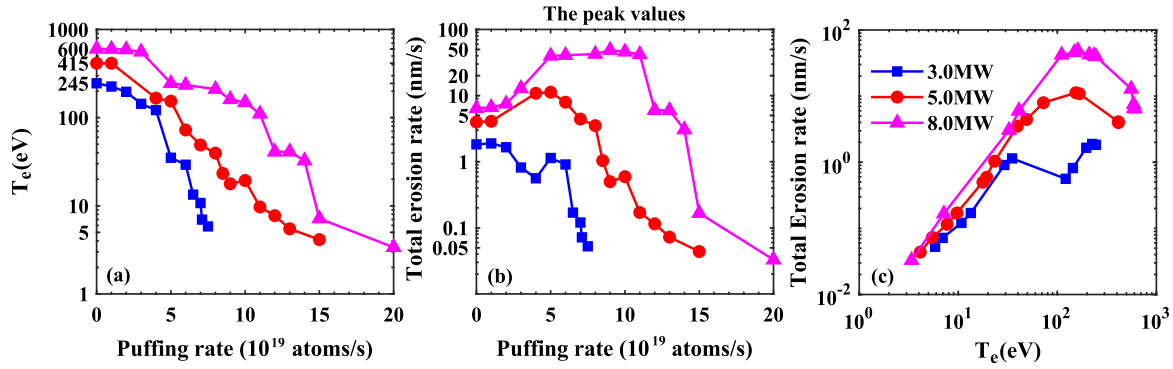

Figure 8. The peak (a) T_e, the peak (b) W erosion rate, as functions of Ne seeding rate and the peak (c) erosion rate as functions of the peak T_e, P_{SOL} = 3.0 MW, 5.0 MW and 8.0 MW, respectively.

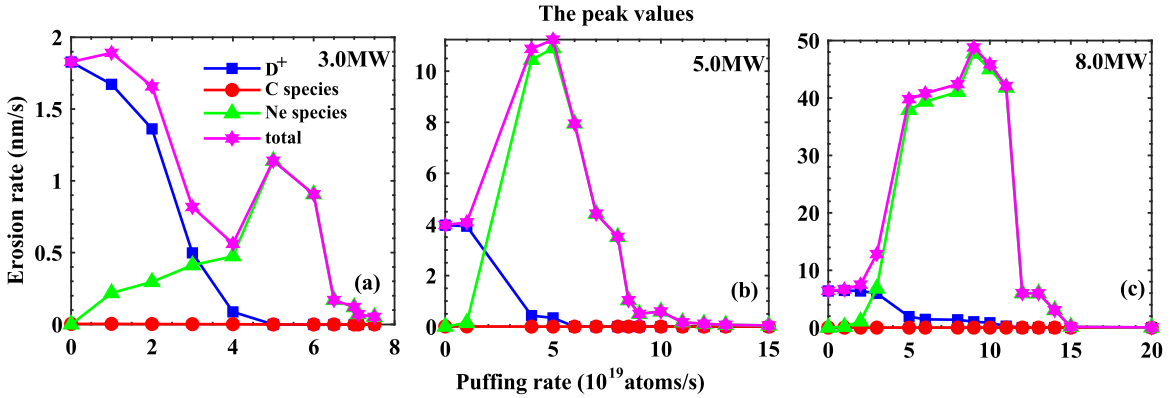

Figure 9. The peak erosion rate, and the erosion by D^+, C ions and Ne ions, as functions of Ne seeding rate, (a) P_{SOL} = 3.0 MW, (b) 5.0 MW and (c) 8.0 MW.

that $R^D_{Ero} \propto \Gamma_{D^+} Y^{D^+}_{Phys,W}$ and $R^{Ne}_{Ero} \propto \sum_{n=1}^{10} \Gamma_{Ne^{n+}} Y^{Ne^{n+}}_{Phys,W}$. During the impurity seeding, the reduction of T_e leads to the decrease of $Y^{D^+}_{Phys,W}$ as well as R^D_{Ero}. The value of R^{Ne}_{Ero} depends on the competition between $\Gamma_{Ne^{n+}}$ and $Y^{Ne^{n+}}_{Phys,W}$. $\Gamma_{Ne^{n+}}$ increases, while $Y^{Ne^{n+}}_{Phys,W}$ decreases as Ne seeding rate increases. When the seeding rate is low, T_e is still high, $\Gamma_{Ne^{n+}}$ plays the dominated role, thus R^{Ne}_{Ero} increases as the seeding rate raises. As the seeding rate further increases, T_e reduces, and $Y^{Ne^{n+}}_{Phys,W}$ plays more and more important role, until to be the dominant factor, and then R^{Ne}_{Ero} decreases as the seeding rate continuously increases. The total erosion rate $R^{total}_{Ero} R^D_{Ero} + R^{Ne}_{Ero}$ is also the competition between R^D_{Ero} and R^{Ne}_{Ero}. When P_{SOL} = 3.0 MW, it is clear that as the seeding rate increases R^{total}_{Ero} decreases due to the reduction of R^D_{Ero}, and then it increases due to the enhance of R^{Ne}_{Ero} (dominated by the raising of $\Gamma_{Ne^{n+}}$), finally it turns to decrease due to the reduction of R^{Ne}_{Ero} (dominated by the decrease of $Y^{Ne^{n+}}_{Phys,W}$). For the higher P_{SOL} (i.e. 5.0 MW and 8.0 MW), the introduction of Ne impurity can significantly increase R^{Ne}_{Ero} when the T_e is not effectively reduced, due to that the sputtering threshold for Ne to W is low. However, in the same condition, the insufficient seeded impurity becomes to the main threat to the lifetime of the W target. Higher P_{SOL} leads to potential higher R^{Ne}_{Ero}, which will become much more critical for future fusion device such as CFETR and DEMO. Only the sufficient impurity seeding can suppress the erosion of the target.

R_{Ero} can be used to evaluate the lifetime of the divertor. It can be seen from figures 10(a)–(b) that the peak particle flux density appears near the OSP. We assume that on EAST the averaged pulse length (T) is 60 s [42], thus divertor R_{Ero} with different Ne seeding rates (0 atoms/s, 9.0 × 10^{19} atoms/s and 2.0 × 10^{20} atoms/s, respectively) under high power discharge (P_{SOL} = 8.0 MW) can be calculated. The total erosion depth (d) is thus expressed as $d = R_{Ero}{}^* n_{shot}{}^* T$, where n_{shot} is the number of discharge shots. The peak erosion depth of three P_{SOL} cases appears near the OSP, and the peak erosion rate is 6.403 nm s^{-1}, 48.792 nm s^{-1} and 0.033 nm s^{-1}, respectively. The thickness of EAST W mono-block is about 5.5 mm from PFS to the water cooling tube [43, 44]. After 1800 shots of discharge, the target erosion distributions are illustrated in figure 10(c). The peak erosion depths (d) are 0.69 mm, 5.27 mm and 0.003 mm, respectively. Clearly, we can observe that the insufficient Ne seeding can greatly reduce the lifetime of the target due to the introducing of the external impurity and the not fully reduced plasma temperature (peak T_e ~ 161.3 eV), whereas the

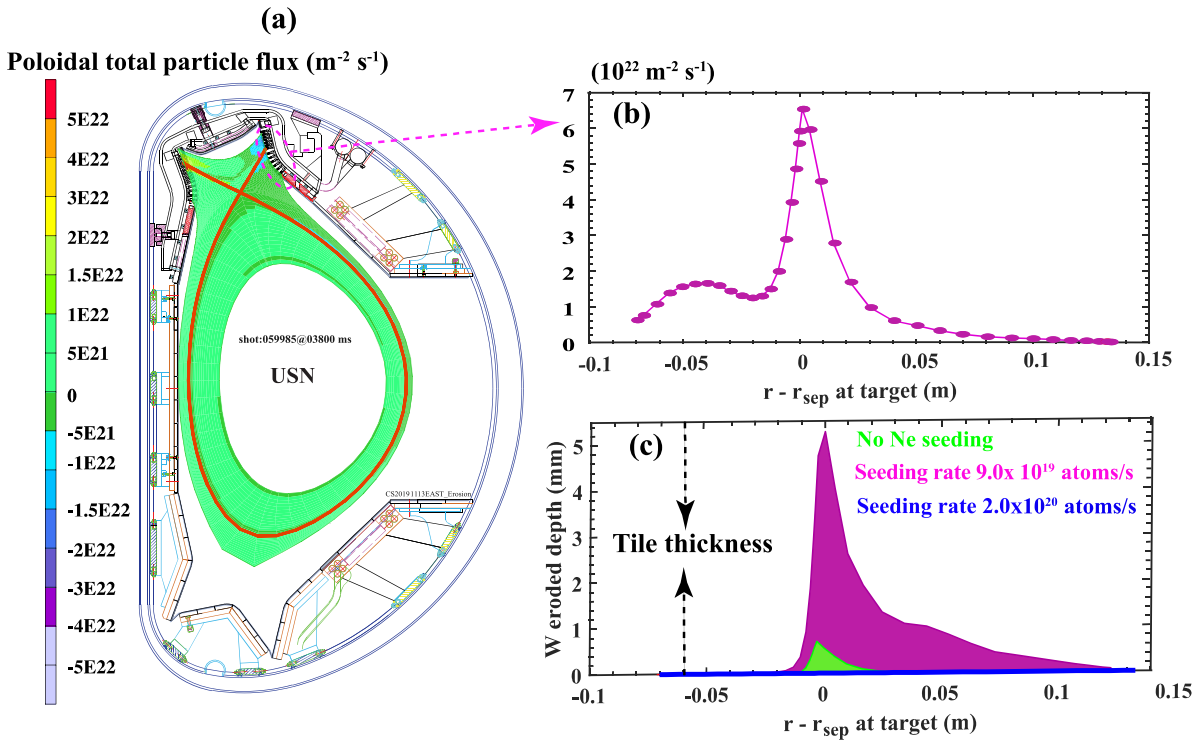

Figure 10. (a) The total poloidal ion flux distribution (Ne puffing rate $= 9.0 \times 10^{19}$ atoms/s and $P_{SOL} = 8.0$ MW), and (b) the flux across the outer target; (c) the estimated outer target erosion depth (the direction is normal to the surface) distribution under different discharge conditions (Ne seeding rate is 0 atoms/s, 9.0×10^{19} atoms/s and 2.0×10^{20} atoms/s, respectively), after 1800 shots. The input power is $P_{SOL} = 8.0$ MW and the averaged pulse length is assumed to be 60 s.

sufficient Ne seeding can fully bring down T_e (<3.4 eV along the target), thus protect the target not to be eroded. The W target can survive for 2.8×10^6 shots with sufficient Ne seeding, compared to 1.4×10^4 shots without impurity seeding, indicating the lifetime can be extended 200 times longer.

The present model does not include W impurity transport calculation, therefore, the W self-sputtering has not been considered. The W self-sputtering induced by sputtered W impurities depends strongly on the incident energy [45]. In the divertor region, the incident energy of W ion is usually below 1 keV, and the corresponding self-sputtering yield is much smaller than 1, therefore, the self-sputtering is negligible in most of the cases [46, 47]. It should be noted that the self-sputtering is also relevant to the incident angle and the roughness of divertor W target. It has been found that the incident angle of the maximum self-sputtering yield is ~80 degree for rough surface and ~60 degree for smooth surface [46, 48]. The different divertor operation regimes can also influence the self-sputtering. For high-recycling regime (HRR) and in partially detached regime (PDR) in pre-ELM cases, it has been reported that the ratio of W content by self-sputtering is ~20% in the HRR and ~8% in the PDR case [49]. In our future work, the self-sputtering will be included because it affects not only the target lifetime or even induces the W self-sputtering avalanche, but also influences the core plasma contamination [50]. The re-deposition has also significant influence on the target lifetime. It can change the net erosion as well as W material property. To simulate the re-deposition, the model should include the divertor plasma physics, the W impurity transport and the dynamic changes of the deposited W layer. However, the present model does not consider last two parts, which may result in the underestimation of the W target lifetime.

4. Conclusion

The erosion of the EAST upper W divertor has been assessed during Ne impurity seeding in different divertor operation regimes by using the SOLPS modeling coupled with the semi-empirical formula for W erosion analysis. The simulation confirms that the external Ne seeding can significantly reduce both the heat flux q and the electron temperature T_e in the divertor region. For the low input power discharge ($P_{SOL} = 1.5$ MW), the impurity seeding is not necessary; while for the medium or high input power ($P_{SOL} \geq 3$ MW), impurity seeding is required to reduce T_e or (and) q. By using the incident energy and particle flux density provided by SOLPS, the W erosion rate by each particle species is assessed. The simulation reveals that during the Ne seeding, the Ne ions play a significant role in the W target erosion, the impact of C ions on the erosion is small, whereas roles of D^+ depends strongly on the P_{SOL} as well as Ne seeding rate. For the Ne-dominant W erosion case, the Ne^{3+} and Ne^{4+} ions contribute to the highest erosion rate. By varying the Ne seeding rate under various P_{SOL}, the W erosion in different conditions is evaluated. The simulation indicates that the total erosion R_{Ero}^{total} depends on the competition between

R^{D}_{Ero} and R^{Ne}_{Ero}, while the value of R^{Ne}_{Ero} is dominated by the competition between $\Gamma_{Ne^{n+}}$ and $Y^{Ne^{n+}}_{Phys,W}$. This causes R^{total}_{Ero} to be greatly enhanced by the insufficient Ne seeding.

The present results indicate that the selection of the impurity seeding rate should be very careful. Although the insufficient seeding gas can reduce the heat flux to the target, R^{total}_{Ero} may be obviously enhanced, which would shorten the target lifetime. This becomes to more critical during high power operation. Only the sufficient impurity seeding can decrease both R^{total}_{Ero} and the heating flux to the target q, thus protect the target. The current erosion calculations are crude, but it provides rapid/effective method to understand total W target erosion under various conditions.

In the future, the heating power will be very high, and the W target erosion may become more and more serious. External impurity seeding is required to cool down the divertor plasma and decrease R^{total}_{Ero}. On one hand, the erosion of W target is important to evaluate the lifetime of the divertor, especially during the designed period of the device such as CFETR. On the other hand, the trace of the sputtered W impurity and understanding its accumulation/distribution/concentration are particularly urgent, which may influence the long-pulse high performance steady-state operation significantly. In the future work, the transport of the eroded high-Z impurities will be investigated during radiative divertor operation with the assistance of the external gas injection. Moreover, the comparison of different novel gas (e.g. nitrogen/neon/argon) by considering the power dissipation and W target erosion will be required. The self-W sputtering and re-deposition should also be included in the model to simulate the erosion accurately.

Acknowledgments

This work is supported by National Key R&D Program of China Nos. 2017YFA0402500, 2017YFE0301206, 2018YFE0301101, 2017YFE0300402 and 2017YFE0300501, National Natural Science Foundation of China under Grant No. 11775044. We thank L Wang (ASIPP) for helpful discussion.

ORCID iDs

Chaofeng Sang https://orcid.org/0000-0002-6861-5242
Rui Ding https://orcid.org/0000-0003-2880-9736
Dezhen Wang https://orcid.org/0000-0003-0517-7318

References

[1] Neu R *et al* 2009 Ten years of W programme in ASDEX Upgrade-challenges and conclusions *Phys. Scr.* **T138** 14038
[2] Neu R *et al* 2013 First operation with the JET international thermonuclear experimental reactor-like wall *Phys. Plasmas* **20** 56111
[3] Brezinsek S, Pospieszczyk A, Sergienko G, Dux R, Cavedon M, Faitsch M and Krieger K 2019 Chemically assisted physical sputtering of Tungsten: identification via the (6)Pi ->(6) Sigma(+) transition of WD in TEXTOR and ASDEX Upgrade plasmas *Nucl. Mater. Energy* **18** 50–55
[4] Kirschner A *et al* 2019 Modelling of tungsten erosion and deposition in the divertor of JET-ILW in comparison to experimental findings *Nucl. Mater. Energy* **18** 239–44
[5] Pitts R A *et al* 2013 A full tungsten divertor for ITER: physics issues and design status *J. Nucl. Mater.* **438** S48–56
[6] Wiesen S, Groth M, Wischmeier M, Brezinsek S, Jarvinen A, Reimold F and Aho-Mantila L 2017 Plasma edge and plasma-wall interaction modelling: lessons learned from metallic devices *Nucl. Mater. Energy* **12** 3–17
[7] Pütterich T, Neu R, Dux R, Whiteford A D, O'Mullane M G and Summers H P 2010 Calculation and experimental test of the cooling factor of tungsten *Nucl. Fusion* **50** 25012
[8] Federici G *et al* 2001 Plasma-material interactions in current tokamaks and their implications for next step fusion reactors *Nucl. Fusion* **41** 1967–2137
[9] Han M K, Wang Z X, Dong J Q and Du H R 2017 Multiple ion temperature gradient driven modes in transport barriers *Nucl. Fusion* **57** 46019
[10] Yang S X, Hao G Z, Liu Y Q, Wang Z X, Hu Y J, Zhu J X, He H D and Wang A K 2018 Toroidal Alfven eigenmode triggered by trapped anisotropic energetic particles in a toroidal resistive plasma with free boundary *Nucl. Fusion* **58** 46016
[11] Sang C, Ding R, Bonnin X, Wang L and Wang D 2018 Effects of carbon impurities on the power radiation and tungsten target erosion in EAST *Phys. Plasmas* **25** 72511
[12] Ivanova-Stanik I, Zagorski R, Voitsekhovitch I and Brezinsek S 2016 Influence of impurity seeding on plasma burning scenarios for ITER *Fusion Eng. Des.* **109** 342–6
[13] Bernert M *et al* 2017 Power exhaust by SOL and pedestal radiation at ASDEX Upgrade and JET *Nucl. Mater. Energy* **12** 111–18
[14] Pitts R A *et al* 2019 Physics basis for the first ITER tungsten divertor *Nucl. Mater. Energy* **20** 100696
[15] Warrier M, Schneider R and Bonnin X 2004 Subroutines for some plasma surface interaction processes: physical sputtering, chemical erosion, radiation enhanced sublimation, backscattering and thermal evaporation *Comput. Phys. Commun.* **160** 46–68
[16] Eckstein W 2008 Sputtering yields *Vacuum* **82** 930–4
[17] Eckstein W 1997 Physical sputtering and reflection processes in plasma-wall interactions *J. Nucl. Mater.* **248** 1–8
[18] Ivanova-Stanik I, Koechl F, Voitsekhovitch I, Telesca G, Zagorski R and Grp E-I-I S M 2014 Integrated core-SOL simulations of ITER H-mode scenarios with different pedestal density *Contrib. To Plasma Phys.* **54** 341–6
[19] Wan B, Li J, Guo H, Liang Y, Xu G, Wang L and Gong X 2015 Advances in H-mode physics for long-pulse operation on EAST *Nucl. Fusion* **55** 104015
[20] Schneider R, Bonnin X, Borrass K, Coster D P, Kastelewicz H, Reiter D, Rozhansky V A and Braams B J 2006 Plasma edge physics with B2-Eirene *Contrib. To Plasma Phys.* **46** 3–191
[21] Reiter D 2009 *The EIRENE Code User Manual Including: B2-EIRENE Interface* pp 1–285
[22] Sang C F, Stangeby P C, Guo H Y, Leonard A W, Covele B, Lao L L, Moser A L and Thomas D M 2017 SOLPS modeling of the effect on plasma detachment of closing the lower divertor in DIII-D *Plasma Phys. Control. Fusion* **59** 25009
[23] Du H, Sang C, Wang L, Bonnin X, Sun J and Wang D 2014 Numerical simulation of the energy deposition evolution on divertor target during type-III ELMy H-mode in EAST using SOLPS *Fusion Eng. Des.* **89** 2461–6
[24] Sang C, Du H, Zuo G, Bonnin X, Sun J, Wang L and Wang D 2016 SOLPS modeling of lithium transport in the scrape-off layer during real-time lithium injection on EAST *Nucl. Fusion* **56** 106018

[25] Zhang C, Sang C, Wang L, Chang M, Liu D and Wang D 2019 Effect of carbon and tungsten plasma-facing materials on the divertor and pedestal plasma in EAST *Plasma Phys. Control. Fusion* **61** 115013
[26] Mao H *et al* 2017 The impacts of lithium and silicon coating on the W source in EAST *Nucl. Mater. Energy* **12** 447–52
[27] Stangeby P C 2000 The plasma boundary of magnetic fusion devices (Bristol: Institute of Physics Publishing)
[28] Yamamura Y, Itikawa Y and Itoh N 1983 Angular dependence of sputtering yields of monoatomic solids *Rep. IPPJ-AM-26*
[29] Sun Z, Sang C, Hu W, Du H and Wang D 2016 Simulation of tungsten erosion and transport near the divertor plate during ELMs by a kinetic method *Fusion Eng. Des.* **109–111** 213–17
[30] Behrisch R and Eckstein W 1986 *Physics of Plasma-Wall Interaction in Controlled Fusion Ed DE Post and R Behrisch* (NY: Plenum) p 413
[31] Eckstein W, Bohdansky J and Roth J 1991 Atomic and plasma material interaction data for fusion *Nucl. Fusion* **1** 51
[32] Eckstein W, Garcia-Rosales C, Roth J and Ottenberger W 1993 *Sputtering data* pp 116–20
[33] Wan B N *et al* 2017 Overview of EAST experiments on the development of high-performance steady-state scenario *Nucl. Fusion* **57** 102019
[34] Wang L *et al* 2019 Advances in plasma–wall interaction control for H-mode operation over 100 s with ITER-like tungsten divertor on EAST *Nucl. Fusion* **59** 086036
[35] Sang C, Guo H, Stangeby P C, Wang H Q, Wang L and Wang D 2020 SOLPS analysis of changes in the main SOL of DIII-D associated with divertor detachment vs attachment and closure vs openness *Nucl. Fusion* **60** 056011
[36] Liu D, Sang C, Wang L and Wang D 2018 The impact of neon-seeding location on the divertor plasma in EAST *Fusion Eng. Des.* **136** 324–9
[37] Jaervinen A E *et al* 2016 Comparison of H-mode plasmas in JET-ILW and JET-C with and without nitrogen seeding *Nucl. Fusion* **56** 046012
[38] Xiang L, Guo H, Wischmeier M, Wu Z, Wang L, Duan Y, Gan K, Shen Y and Chen Y 2017 Investigation of the effects of impurity seeding under different magnetic configurations in L-mode plasma in EAST tokamak *Phys. Plasmas* **24** 92514
[39] Ding F *et al* 2019 Plasma–tungsten interactions in experimental advanced superconducting tokamak (EAST) *Tungsten* **1** 122–31
[40] Zagórski R, Gałazka K, Ivanova-Stanik I, Stępniewski W, Garzotti L, Giruzzi G, Neu R and Romanelli M 2017 Numerical analyses of baseline JT-60SA design concepts with the COREDIV code *Nucl. Fusion* **57** 066035
[41] Stangeby P C and Leonard A W 2011 Obtaining reactor-relevant divertor conditions in tokamaks *Nucl. Fusion* **51** 063001
[42] Luo G N *et al* 2017 Overview of decade-long development of plasma-facing components at ASIPP *Nucl. Fusion* **57** 065001
[43] Yao D M *et al* 2016 Design, R&D and commissioning of EAST tungsten divertor *Phys. Scr.* **2016** 14003
[44] Wang B, Zhu D, Ding R and Chen J 2017 Thermal analysis on the EAST tungsten plasma facing components with shaping structure counteracting the misalignment issues *Plasma Sci. Technol.* **19** 025603
[45] Shoji M, Kawamura G, Masuzaki S and Morisaki T 2018 Impurity transport simulation in the peripheral plasma in the large helical device with tungsten closed helical divertor *Nucl. Mater. Energy* **17** 188–93
[46] Salonen E, Nordlund K, Keinonen J and Wu C H 2003 Molecular dynamics studies of the sputtering of divertor materials *J. Nucl. Mater.* **313–316** 404–7
[47] Yamoto S, Bonnin X, Homma Y, Inoue H, Hoshino K, Hatayama A and Pitts R A 2017 Kinetic modeling of high-Z tungsten impurity transport in ITER plasmas using the IMPGYRO code in the trace impurity limit *Nucl. Fusion* **57** 116051
[48] Drobny J and Curreli D 2018 F-TRIDYN simulations of tungsten self-sputtering and applications to coupling plasma and material codes *Comput. Mater. Sci.* **149** 301–6
[49] Wang F *et al* 2018 Simulations on W impurity transport in the edge of EAST H-mode plasmas *Plasma Phys. Control. Fusion* **60** 125005
[50] Chankin A V, Coster D P and Dux R 2014 Monte Carlo simulations of tungsten redeposition at the divertor target *Plasma Phys. Control. Fusion* **56** 025003